JOURNAL OF GEOPHYSICAL RESEARCH, VOL. 102, NO. D13, PAGES 16,011-16,022, JULY 20, 1997

Detection of tropospheric OH radicals by long-path differential-optical-absorption spectroscopy: Experimental setup, accuracy, and precision

Martin Hausmann, Uwe Brandenburger, Theo Brauers, and Hans-Peter Dorn

Institut für Atmosphärische Chemie, Forschungszentrum Jülich, Jülich, Germany

Abstract. This paper describes a newly developed long-path differential-optical-absorption-spectroscopy instrument used for the measurement of tropospheric OH radicals. The instrument consists of a high resolution echelle spectrometer in conjunction with a multiple-reflection cell of 38.5 m base length and a UV laser light source that provides a spectral line width of 0.41 nm. Local in situ absorption measurements at total path lengths of either 1.85 or 3.1 km can be performed. The simultaneous observation of six atmospheric OH rotational absorption lines ($Q_1(2)$, $Q_{21}(2)$, $R_2(2)$, $Q_1(3)$, $Q_{21}(3)$, and $P_1(1)$) around 308 nm allows OH measurements with high specificity. A new method to accurately determine the precision and the detection limit of each individual OH measurement data point is presented. Presently, a 2σ-detection limit of 1.5×10^6 OH cm^{-3} is achieved (based on 1.85 km absorption path length and about 6 min integration time), which corresponds to a minimum detectable optical density of 2.5×10^{-5}. The absolute instrumental accuracy was calculated to be better than 6.5%, which emphasizes the qualification of the long-path absorption technique as an absolute method. Examples of field experiments are reported to illustrate the present performance.

1. Introduction

The determination of the concentration of hydroxyl radicals (OH) in the atmosphere is central to the understanding of atmospheric photochemistry. OH radicals are the driving oxidizing agent initiating the removal of most atmospheric trace gases. Maximum OH concentrations in the troposphere are about 1×10^7 molecules cm^{-3} corresponding to a mixing ratio of only about 0.4 parts per trillion by volume (pptv). A review of the importance of OH to atmospheric chemistry can be found elsewhere [see, e.g., *Hewitt and Harrison*, 1985, *Ehhalt et al.*, 1991]. Accurate measurements of the very weak and highly variable concentrations of tropospheric OH radicals are still very sparse, although necessary for a quantitative understanding of the self-cleansing capacity of the atmosphere and its potential change due to anthropogenic emissions.

For the last 2 decades various methods, including both direct and indirect techniques, have been applied to determine the atmospheric concentration of OH radicals, which gave the basic understanding of its abundance and of its significance to atmospheric chemistry. The performance of the diverse OH measurement techniques was previously reviewed by *Crosley* [1994]. Although most of these detection techniques are very sensitive, there are objections to some for not being direct, absolute, specific, or in situ, respectively. The only absolute and direct in situ method that is presently applicable to OH measurements is the long path absorption technique [see, e.g., *Hofzumahaus et al.*, 1991].

Long-path differential-optical-absorption-spectroscopy (LP-DOAS) is a well established technique for the tropospheric measurement of OH and other trace gases (like NO_3, BrO, IO, HCHO, HNO_2, O_3, NO_2, and SO_2 [see, e.g., *Platt and Perner*, 1980; *Platt and Hausmann*, 1994]). First tropospheric OH measurements based on high resolution laser LP-DOAS were performed by *Hübler et al.* [1984]. Meanwhile, the same and other authors have reported LP-DOAS OH measurements in the troposphere [*Perner et al.*, 1987; *Callies*, 1988; *Dorn et al.*, 1988; *Platt et al.*, 1988; *Hofzumahaus et al.*, 1991; *Mount*, 1992; *Armerding et al.*, 1994; *Dorn et al.*, 1996]. LP-DOAS makes use of the extinction of a light beam in the free troposphere (of typical 2 to 10 km path length) by the specific absorption of the trace gases under observation. It allows to perform absolute and calibration-free in situ measurements based on the spectral properties of the investigated molecules (OH, SO_2, HCHO, $C_{10}H_8$, etc.).

The specific light absorption by a trace gas is quantitatively described by Lambert-Beers law,

$$D'(\lambda) = \ln\left(\frac{I_0(\lambda)}{I(\lambda)}\right) = c\,\sigma'(\lambda)\,L \qquad (1)$$

where $I_0(\lambda)$ and $I(\lambda)$ are the light intensities (at a wavelength λ) without absorption and with absorption, respectively, $D'(\lambda)$ denotes the differential optical density, $\sigma'(\lambda)$ is the differential absorption cross section of a specific absorption band of a trace gas, c is the concentration of the absorbing trace gas (e.g., OH, SO_2, or HCHO), and L is the absorption path length. Since $I_0(\lambda)$ is unknown in differential absorption spectroscopy it is calculated by interpolation from the off-line light intensities [see *Platt*, 1994]. To make sure that a certain trace gas accounts for the observed absorption, a reference absorption spectrum of the pure trace gas is usually fitted to the measured atmospheric spectrum by a least squares fit, and the optical density is determined from the fitted reference spectrum. For a detailed description of the procedure the reader is refered to *Dorn et al.* [1992, 1995b].

Paper number 97JD00931.
0148-0227/97/97JD-00931$09.00

For weak absorption lines the precision of LP-DOAS measurements depends on the spectral evaluation procedure. In principle, the measurement precision is limited by the shot noise of the sampled photo electrons. In practice, usally sufficient light is sampled so that the shot noise limitation becomes small compared to another limiting effect. This is given by the occurrence of spectral structures that interfere with the characteristic absorption spectrum of OH. These interferences are both real absorption structures of not yet identified atmospheric trace gases and in a great part nonreproducible artificial structures that are generated within the optical setup itself. The latter effect limited the measurements of the earlier instruments to minimum optical densities of typically $(2\text{-}4)\times10^{-4}$ thus necessitating long absorption path lengths. For example, to detect 5×10^{6} OH molecules cm^{-3}, an absorption path length of more than 4 km was needed (taking $\sigma(OH) = 1.0\times10^{-16}$ cm^2, see equation (1)). Thus the measurements resulted in spatially integrated OH concentration values along the extended path. This "nonlocality"-characteristic was the main disadvantage of the earlier long light path arrangements since the OH concentration is spatially variable. In order to intercompare LP-DOAS results with results of alternative direct in situ measurement techniques (like-laser induced fluorescence (LIF)), and to enable a meaningful interpretation of the observed OH concentrations by model calculations, localized LP-DOAS measurements should be carried out.

We describe a new LP-DOAS setup for tropospheric OH measurements that was designed to overcome the disadvantages of a spatially extended light path and to reduce irregular spectral interferences. Furthermore, we developed new methods to determine the instrumental accuracy and the precision of an OH concentration data point derived from an individual spectrum.

2. Experimental Setup

The electronic transitions between rotational states of the vibrational ground state and the vibrational ground state of the first excited electronic state of OH at 308 nm ($X^2\Pi$ (v''=0) $\rightarrow$ $A^2\Sigma^+$(v'=0)) are used for the OH detection by absorption (see Figure 1). Because the typical absorption line width under tropospheric conditions is about 2.5 picometer (pm) [*Dorn et al.*, 1995a], a high spectral resolution is necessary. The instrumental setup described here is a new development based on experiences with earlier designs [*Callies*, 1988; *Dorn et al.*, 1992]. An overview drawing of the new setup is shown in Figure 2. The instrument consists of eight major components: (1) a broadband laser light source providing a spectral output at 616 nm, (2) a frequency doubler unit (BBO) to generate the ultraviolet light necessary for OH detection, (3) transfer optics adapting the laser beam to the multiple-reflection cell, (4) an improved open multiple-reflection cell (MRC) which allows to install a wall free atmospheric absorption light path of more than 3 km length, (5) special imaging optics to perform a stable illumination of the entrance slit of the spectrograph, (6) a high-resolution Echelle spectrograph unit with a linear dispersion of 0.01 nm/mm, (7) a photo diode array (PDA) detector for the simultaneous observation of a spectral interval of 0.26 nm which comprises 6 OH absorption lines (Figure 1), and (8) computer hardware and software tools to control the instrument.

2.1. Laser Light Source

A light source used for LP-DOAS technique needs to fulfill three important requirements: (1) a broadband emission for simultaneous measurement of more than one specific absorption line, (2) a sufficiently high spectral luminance within the spectral range under observation, and (3) the absence of spectral intensity modulations within the spectral emission profile. All 3 requirements can be met by the use of a mode-locked picosecond laser as a light source.

We apply a commercial laser system consisting of a dye laser (Spectra Physics, model 3500) synchronously pumped by a mode-locked, frequency-doubled Nd:YAG laser (Spectra Physics, model 3800S) at a repetition rate of 82 MHz. This arrangement provides a Gaussian dye laser emission profile at 616 nm with a

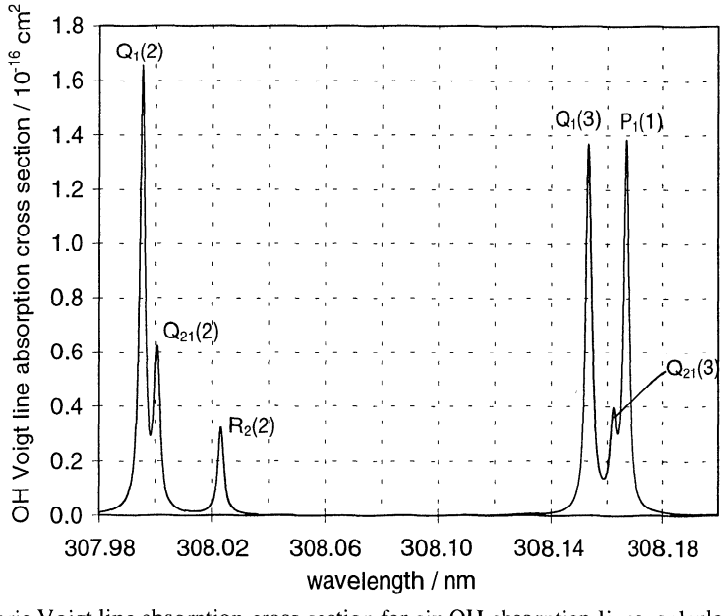

Figure 1. Tropospheric Voigt line absorption cross section for six OH absorption lines, calculated from *Dorn et al.* [1995a] at 1010 hPa and 298 K valid for infinite spectral resolution).

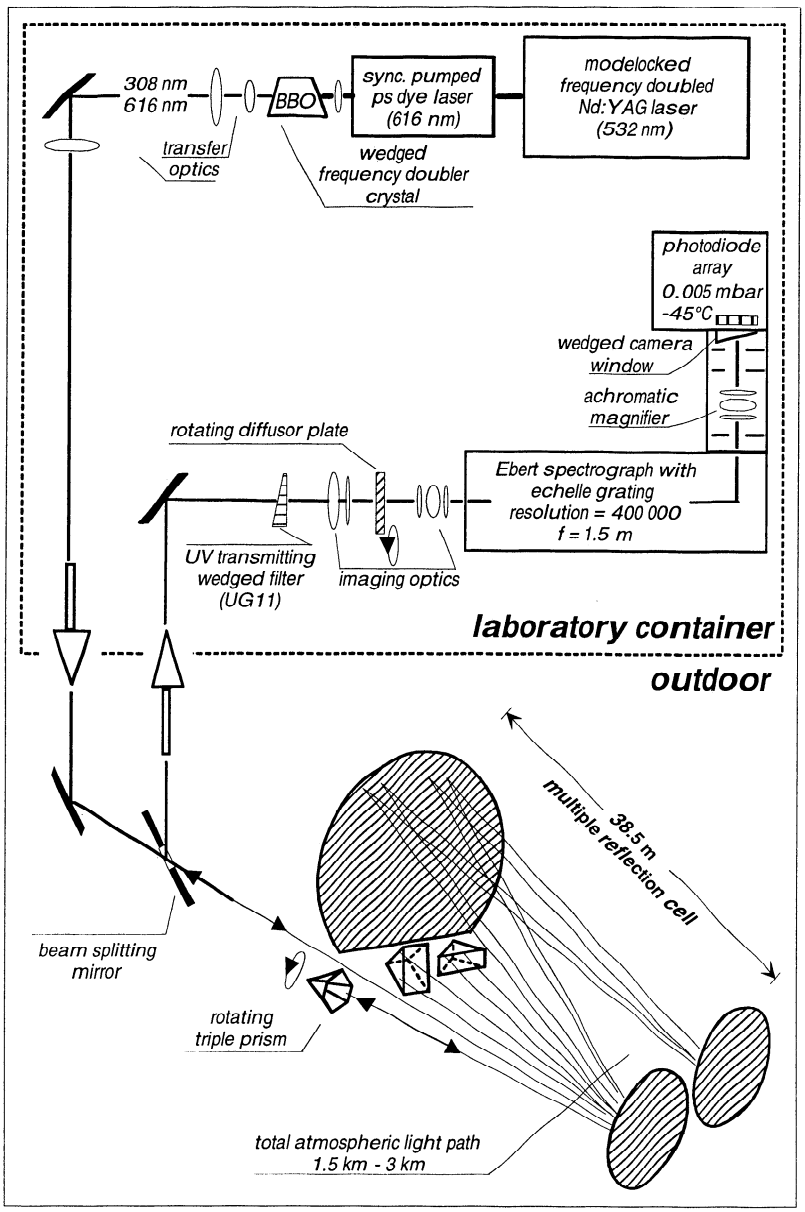

Figure 2. Scheme of the LP-DOAS instrument comprising a laser light source, open path multiple-reflection cell, and a high resolution Ebert type spectrograph linked to a photo diode array.

spectral line width of about 0.82 nm full width at half-maximum (FWHM) and an output power of 250 to 400 mW. Assuming the line width is determined by Fourier theory, it corresponds to output pulses of less than 1 ps duration.

To convert the 616-nm dye laser output to 308 nm, the beam is focused into an angle-tuned Beta Barium Borate (BaB_2O_4 (BBO), length 7 mm) frequency doubler crystal by a f = 60 mm spherical lens. Although BBO posseses only a poor conversion efficiency (< 2%, under these specific operating conditions), it has the advantage of broadband conversion. The resulting spectral profile shows a FWHM of about 0.41 nm, considerably broader in comparison to the spectral range under observation (see Figure 3).

2.2. Transfer Optics

The transfer optics between the BBO crystal and MRC consists mainly of two plano-convex lenses arranged as beam expander with focus adjustment. This arrangement allows to focus the beam on the entrance of the MRC and the adaption of the focus diameter (around 3 mm) and the divergence (around 4 mrad) to the specific optical requirements of the MRC. Thus the total laser output (at 308 nm) can be used without geometrical light loss. Also, a portion of the nearly colinearly emitted fundamental wavelength (616 nm) is directed to the MRC for the alignment of the optical components.

2.3. Compensation Multiple-Reflection Cell (MRC)

Armerding et al. [1992] first applied open path multipass absorption to OH measurements in the troposphere by combining their "fast scanning laser technique" to a 6-m base length MRC. We operate a White-type MRC [*White*, 1976] which was further improved using the modifications by *Ritz et al.* [1992]. It is a 38.5-m base length system with two collimator mirrors of 150

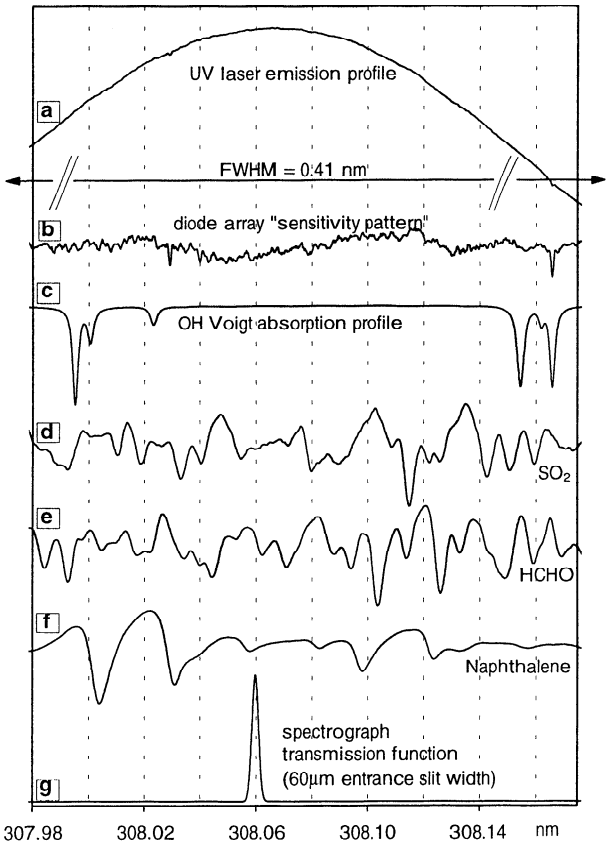

Figure 3. Spectral functions relevant to tropospheric OH measurements by the LP-DOAS instrument note that the zero points of the individual curves are suppressed): (a) Gaussian spectral intensity distribution of laser light source, (b) "broadband" spectral features caused by laser fluctuations and "small band" spectral features caused by the pixel-pixel sensitivity variation of the PDA overlaying the Gaussian spectral intensity distribution (10 times magnified), (c) pure tropospheric Voigt OH absorption profile adapted from the cross sections in Figure 1, (d-f) reference cell spectra of the interfering species SO_2, HCHO, and $C_{10}H_8$ (as measured by the instrument), and (g) spectrograph transmission function (FWHM = 3.3 pm) as used for numerical simulations (see text).

mm in diameter and a field mirror of 200 mm in diameter (with a reflectivity of 99.0% at 308 nm).

Major problems in utilizing a long absorption path length in the free atmosphere are beam wander (caused by vertical atmospheric temperature gradients) and beam broadening (caused by atmospheric turbulence). To overcome these problems the laser beam is directed twice through the MRC: The regular exit beam of the White design is reflected into the MRC by a rotating triple prism (free aperture 20 mm). Thus the beam travels the complete passage a second time precisely along the actual trace of the first passage but in reverse direction. Therefore all beam deformities and corresponding imaging errors are almost perfectly compensated. While traveling the second passage the focal spot diameter of the beam does not increase any further even for the long light path of 3 km. This observation clearly demonstrates the compensation effect of the present MRC construction.

As a consequence of this arrangement an overlay of the entrance spot and the exit spot is formed. However, the diameter of the exit spot is much larger than the diameter of the entrance spot (typically 15 to 20 mm exit spot size in comparison to 3 mm entrance spot size, due to beam displacement by the rotating triple prism and the subsequent weak miscompensation of the beam deformity). It allows to separate the exit beam from the entrance beam by a mirror with a 3-mm hole at its center which is placed in the focal plane of the MRC. The specific construction of this MRC allows to set up light path lengths of 616, 1848, and 3080 m.

The use of a MRC of 38.5-m base length provides feasibility to perform long-path absorption measurements within a small air volume. Taking into consideration fast OH chemistry with HO_x lifetimes of a minute and wind speed of a few meters per second, the spatial "locality" of the measurements is maintained.

2.4. Stabilizing Imaging Optics

After leaving the MRC, the laser beam is directed to a lens-diffuser combination that creates a homogeneous illumination of the entrance slit of the spectrometer and, as a consequence, of the photo diode array detector. This is the most significant property of the imaging optics since a stable and uniform illumination of the grating and the PDA detector is the essential condition for a successful suppression of the sensitivity pattern of the PDA [*Dorn et al.*, 1995b] (section 2.6). In detail the imaging optics comprise three parts. A group (f = 70 mm) of two planoconvex quartz lenses forms an intermediate image on a quartz diffuser plate which diffuses 50% of the light within a 30° cone (full angle). The diffuser plate rotates (10 to 50 rps) around the beam axis in order to smooth out the speckle pattern generated by the diffuser plate. Finally, a three-lens group (f_{total} = 12 mm) of two planoconvex quartz lenses and one biconvex quartz lens images the spot on the diffuser plate onto the entrance slit of the spectrograph. The overall result of that optical design is a geometrically stable light spot at the entrance slit of the spectrograph with a diameter of about 300 µm.

2.5. High Resolution Spectrograph

A high dispersion spectrograph is needed to resolve tropospheric OH line widths of 2.5 pm. We use a commercial 1.5-m focal length Ebert-type f/13 spectrograph (SOPRA UHRS F1500) equipped with an Echelle grating (Milton Roy, blaze wavelength 5.631 µm) with 316 grooves/mm operating in 18th order (at 308 nm) providing a linear dispersion of 0.05 nm/mm. Furthermore, a three lens achromatic 5-times magnifier images the exit plane of the spectrograph onto a PDA detector. Hence a corresponding linear dispersion of about 0.01 nm/mm is achieved. The measured spectral resolution of the spectrograph is 420,000 (without consideration of the influence of the PDA [*Brandenburger* 1992] at an entrance slit width of 15 µm (the final spectral resolution used is discussed in section 3.2). For field measurements an entrance slit width of 60 µm was chosen as an optimum between spectral resolution and transmitted light intensity (see section 3.2). As a result, the spectral resolution of the spectrometrical system (the combination of entrance slit, spectrograph, magnifier, and PDA detector used) is about 91.000 corresponding to 3.3 pm.

For high sensitive DOAS operation, certain additional attributes of the spectrograph are important. Because extremely weak spectral intensity variations are investigated, internal stray light, reentry spectra, and "ghosts" must be suppressed to a sufficient extend. Therefore proper masks and irises were assembled to block stray light and reflections of the optical

components (like the lenses and the PDA surface). Another important aspect is the height of the entrance slit of the spectrograph. Because the entrance slit is imaged onto the PDA by the spectrograph, the slit height determines the illuminated sector of the PDA (and thus its actual diode-to-diode sensitivity; see section 2.6). For the present configuration we mounted a mask (slit, 200 μm width) on the entrance slit that defines a certain height of illumination on the PDA. Owing to the astigmatism of the Ebert spectrograph, the actual height of the spectrum on the PDA is about 1.5 mm (note that the dimensions of the entrance slit are imaged 5 times magnified onto the PDA detector).

2.6. Photo Diode Array (PDA)

The usage of a PDA for DOAS application holds for three major advantages: (1) simultaneous observation of a broad spectral range, (2) the multiplex effect, and (3) the independence of the measured atmospheric absorption structure from intensity fluctuations caused by atmospheric turbulence while recording a spectrum. Here a windowless 1024 element self-scanning linear PDA (Reticon RL1024 SAU) is mounted in a vacuum tight housing behind a wedged quartz window (3° wedge angle). The housing allows to evacuate the PDA environment to 0.005 mbar in order to cool the PDA down to -45°C by a two stage Peltier cascade without water condensation. To avoid illumination of the on-chip switching transistors and shift registers of the PDA, a mask was placed in front of the PDA surface. The PDA is operated by a 16-bit controller (Princeton Instruments ST1015) connected to a PC.

The clear disadvantage of a diode array detector in comparison with a "scanning spectrograph-single detector" system is the diode-to-diode sensitivity variation ("sensitivity pattern") which is typically of the order of 1% of the measured signal. Thus the instrumental pattern is up to 3 orders of magnitude stronger than the absorption signal of tropospheric OH radicals which are between 0.001 and 0.05% of the measured signal. Therefore it is necessary to remove the sensitivity pattern from the absorption spectra.

It is a usual practice to perform a PDA-reference record without trace gas absorption subsequently to the atmospheric absorption measurement in order to calibrate the actual relative PDA sensitivity [*Dorn et al.*, 1992]. However, we have found that this procedure is imperfect because the exact sensitivity pattern of the diode array depends on the angle of incidence and on the light intensity distribution across the photosensitive area of a particular photo diode. In practice, an identical illumination of the diode array for both the atmospheric measurements and calibration measurements cannot be realized. Thus successive calibration is an inadequate method. We have developed the so-called multi-channel scanning technique (MCST) which allows to determine the atmospheric trace gas absorption signal as well as the actual PDA sensitivity pattern for every single measurement spectrum. A detailed description of this technique was published by *Brauers et al.* [1995].

2.7. Combined Features of the Instrumental Setup

Around 308 nm a spectral section of 0.26 nm width can be simultaneously recorded by the PDA (Figure 3). Thereby the FWHM of the OH lines is sampled by about 16 detector channels (at 60-μm entrance slit width). Since the spectrographical system influences the line shape of the observed absorption lines the spectrograph transmission function (STF) has to be considered. The STF describes the combined effect of a number of instrumental features: the entrance slit, the spectral resolution of the diffraction grating, the optical imaging qualities, and the specific properties of the PDA detector. To determine the STF, a sufficient narrow emission line within the spectral range under investigation is usually recorded by the spectrograph. Since a narrowband line source of FWHM ≤ 0.2 pm near 308 nm was not available, we recorded the STF at 632.8 nm taking a He-Ne laser. Actually, the resolution of our spectrograph system even at very small entrance slit is not limited by the resolution of the grating (neither at 308 nm nor at 633 nm) but by the pixel to pixel distance of the PDA (25 μm) and by spherical aberrations due to the off-axis characteristics of the spectrograph imaging optics. Both are pure geometrical quantities. Figure 3 (bottom trace) shows the record of the STF for an entrance slit of 60 μm width. It has a slightly asymmetric line shape with a FWHM of about 13.3 PDA pixels, corresponding to the (5-times magnified) image of the 60 μm entrance slit. This high spectral resolution in combination with the broad spectral range of observation enables to distinguish very well the specific OH absorption and overlapping absorption features of other trace gases like SO_2 or HCHO (see Figure 3). The influence of the STF on the observed absorption line shapes is demonstrated in section 4.1.

The MRC in conjunction with the new spectrograph entrance optics provide a sufficiently stable illumination of the PDA. In combination with the multi-channel scanning technique [*Brauers et al.*, 1995] this arrangement allows the detection of optical densities as low as 2×10^{-5} (see section 5). This corresponds to an improvement of about a factor 10 compared to the former DOAS instrument [*Dorn et al.*, 1988]. Attention was paid to optimize the surface properties of the installed optical components. All mirrors are coated with dielectric layers to enhance reflectivity, and all lenses carry antireflection coatings for 308 nm to minimize etalon-type interference effects. The operation of the whole instrument including path length setting of the MRC, wavelength setting of spectrometer, signal filtering, and spectra deconvolution is completely controlled by the PC program MFC [*Gomer et al.*, 1993].

3. Optimization of the Instrument

In theory, the detection limit is determined by the Poisson statistics of the sampled photons. The photon flux onto the PDA is a function of entrance slit width and absorption path length. Since the setting of these parameters influence the total light flux and the absorption signal strength, we have looked for the best compromise between photon flux on the one hand and large absorption path length and high spectral resolution on the other.

3.1. Absorption Path Length

In order to achieve the lowest possible detection limit at a given signal integration time, the number of passes of the MRC can be optimized. There are two counteracting effects which determine the optimum number of passes: The longer the path length (higher number n of passes) the stronger the absorption signal, but the higher the light losses and, consequently, the lower the signal-to-noise-ratio (SNR). According to *Ritz et al.* [1992] this dependence of the SNR can be expressed as

$$SNR \sim (n+2)\,(RT)^{n/2} \qquad (2)$$

where n is the number of passes through the MRC, R is the reflectivity of the MRC mirrors, and T is the atmospheric transmittivity per MRC base length. Using R = 99% (present

mirror coating) and T ≈ 98.5% (due to the total light extinction by 50 ppbv ozone, Rayleigh scattering, and Mie scattering for typical continental aerosol distributions), the SNR peaks for n ≈ 75, corresponding to a total path length of 2900 m. Since the SNR (equation (2)) in the vicinity of its peak value is a flat function of n, the pathlength can be optimized under consideration of secondary criteria. For instance, if the stability of the optical alignment of the MRC setup is subjected to thermal drifts, a shorter path length can be chosen. As mentioned above, the measurement limit is often not determined by shot noise (and thus not by Poisson statistics) but by irregular spectral structures. In this case the number of passes can be enhanced as long as the theoretical limit (equation (2)) or the technical maximum number of passes is reached (for our present configuration $n_{max} = 80$).

3.2. Spectral Resolution

To achieve the best detection limit, the spectral resolution (entrance slit width of the spectrometer) can be optimized. There also are two opposing effects: If the entrance slit width is enlarged to increase the light throughput and thus the SNR, the spectral resolution decreases and thus the effective absorption cross section σ_{EFF} [*Dorn et al.*, 1995a]. Assuming Gaussian shaped line profiles, this relation with respect to SNR can be approximately summarized as

$$SNR \sim \sqrt{\frac{\Delta\lambda}{G^2 + (\Delta\lambda)^2}} \qquad (3)$$

where $\Delta\lambda$ is the spectral resolution (in picometers) and G is the FWHM of absorption line profile. The SNR reaches a maximum for $\Delta\lambda = G$. Thus, for tropospheric OH measurements, the optimum spectral resolution is 2.5 pm. For this instrument a resolution of about 3.3 pm was chosen as a result of an empirical optimization. Therefore the present choice of spectral resolution and absorption path length gives the best signal-to-noise ratio for OH-long path absorption measurements under typical continental tropospheric conditions.

4. Error Considerations

4.1. OH Absorption Cross Section and Instrumental Accuracy

The accuracy of LP-DOAS mainly depends on the accuracy of the OH absorption cross section used [*Dorn et al.*, 1995a]. Because the LP-DOAS method claims to be an absolute method, a well-defined absorption cross section, valid for the particular instrument, is needed. The corresponding cross sections for the pure Voigt absorption profile under tropospheric conditions used here were calculated according to *Dorn et al.* [1995a]. The OH Voigt profile as calculated from fundamental quantities cannot be observed since the analyzing spectrograph, having a spectral resolution close to the OH Voigt line width, will significantly broaden the line shape and consequently reduce the line strength.

Here we describe the impact of the spectrograph transmission function (see section 2.7) and the spectral scanning and filtering technique (used for the data generation) on the calculated Voigt OH line shape. Finally, the resulting calculated absorption spectrum is compared with an in situ recorded OH reference spectrum in order to test the validity of these calculations. The impact on the absorption cross section is calculated for the strongest tropospheric OH line ($Q_1(2)$, line center at 307.9951 nm). Figure 4a shows a Voigt absorption spectrum calculated after *Dorn et al.*, [1995a]. Here the $Q_1(2)$ line strength is set to 100% corresponding to a cross section at the line center of 1.72×10^{-16} cm^2 (for 290°K and 998.5 hPa), which already consideres the overlap of the $Q_{21}(2)$ line. Figure 4b shows the broadened OH line resulting from the convolution of the absorption spectrum in Figure 4a with the spectrograph transmission function. The experimentally observable line strength for the $Q_1(2)$ transition becomes reduced by about 35%. Figure 4c shows an additional modification by the multi channel scanning technique (MCST) as described by *Brauers et al.* [1995]. The performance of this technique results in a slight but well defined broadband modification of the OH spectrum which leads to a further reduction of the OH cross section by 7.2%. Figure 4d shows the effect of the subsequent treatment by a high pass filtering procedure which is necessary to remove broadband modulatiuons which frequently occur in atmospheric spectra. Here the spectrum was divided by a polynomial fit of the third order. Thus the OH spectrum undergoes a further modification leading to a negligible reduction of the cross section by about 0.01%. Overall, the spectral features of the OH lines are

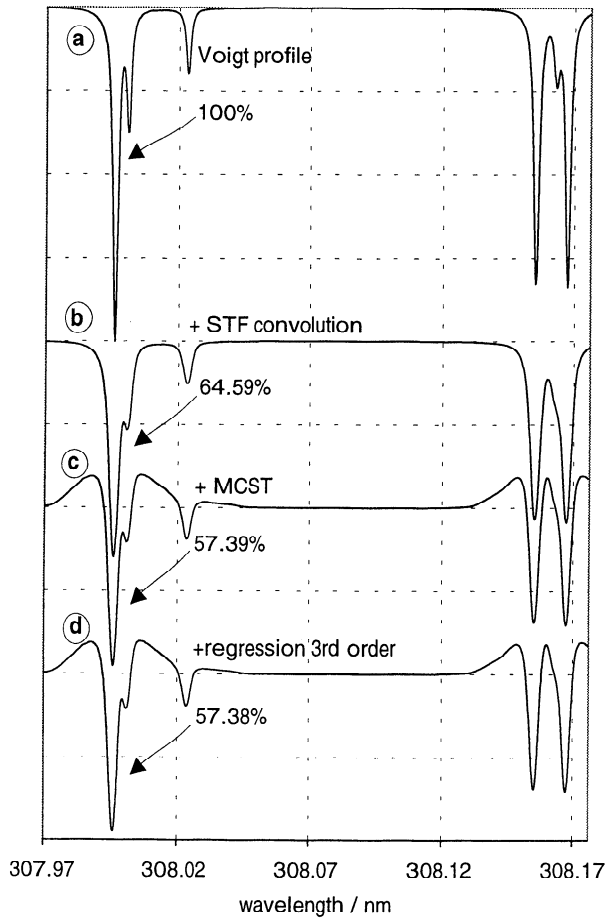

Figure 4. Calculation of a theoretical tropospheric OH absorption spectrum valid for the experimental setup (relative units). Percentage values indicate the reduction of the ($Q_1$2) line strength relative to the pure Voigt profile: (a) calculated pure Voigt OH absorption spectrum (p. Figure 1); initial line strength of the $Q_1(2)$ line is set 100%, (b) simulated impact of the spectrograph transmission function (STF) on the Voigt OH profiles, (c) influence of spectral modification by the multi channel scanning technique, and (d) the effect of high pass filtering (see text).

modified, and the $Q_1(2)$ cross section at the line center is reduced to $\sigma_{eff} = 9.87 \times 10^{-17}$ cm^2 (corresponding to 57.4% of its original value).

Testing the validity of the numerical calculations described above is easily achievable by a comparison of this spectrum with an in situ measured OH reference spectrum. This test was performed in a field study by illuminating the air volume close to the field mirror of the MRC by a low pressure mercury lamp. Photolyses of ambient water vapor at 185.9 nm leads to the formation of high OH radical concentrations. The OH spectrum was recorded by applying MCST. Figure 5 shows a superposition of the recorded spectrum and the calculated spectrum fitted (scaled) to the recorded spectrum. Both spectra were subjected to a high pass filtering procedure. Here a regression of ninth order was applied since both spectra were fitted without an additional polynomial (as usually performed in spectra evaluation procedures). The difference of the measured and the calculated OH spectrum is shown in Figure 5.

A number of systematic errors accounts for the small remaining discrepancy which, however, cannot be quantified in detail. Nevertheless, the total error on the line strength can be calculated. In Figure 5 this error is evaluated for the $Q_1(2)$ line.

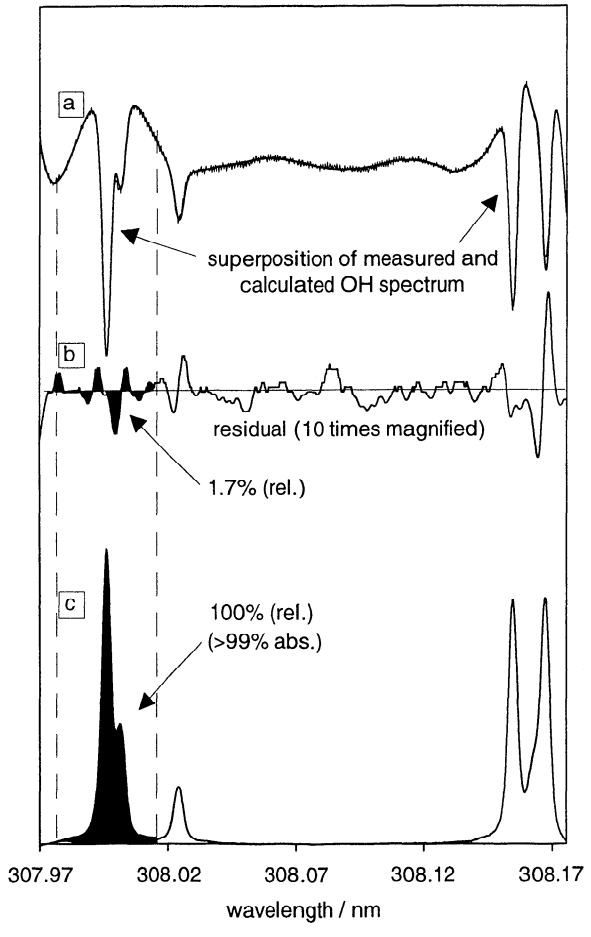

Figure 5. a) Comparison of calculated and measured tropospheric OH line profiles to determine the error of the absorption cross section caused by line shape failure. A calculated OH absorption spectrum is superimposed by the scaled in situ reference record of OH. (b) The difference of the two spectra after removing the high frequent noise) is about 1.7% of (c) total line strength for $Q_1(2)$ line.

Table 1. List of Systematic Errors Limiting the Instrumental Accuracy

Type of Error	Contribution, %
OH reference line shape	<1.7
Total line strength	≈3.0
Atmospheric pressure change	<1.0
Multi-channel scanning technique	<0.3
Absorption path length	<0.5
Total systematic error (accuracy)	<6.5

The total area of deviation (sum of all solid contours in Figure 5, middle trace) is related to the total line strength of the $Q_1(2)$ line (solid contours in Figure 5, bottom trace) yielding a corresponding contribution of only 1.7%. This is a conservative estimate, since the line strength error was calculated by the sum of absolute deviations (solid contours, middle trace), not by the sum of positive and negative values. Thus we conclude that the relative error by line shape is <1.7%.

Besides the relative uncertainty of the line shape, further contributions to the total error of the absorption cross section have to be considered (Table 1). *Dorn et al.* [1995a] noticed that integrated cross section values of the OH lines as discussed in literature vary by about 3% (whereby the corresponding 1σ precisions of the individual values given in literature are less than 1.5%). Changes of atmospheric pressure will cause a slightly variable line broadening during the field measurements resulting in a corresponding uncertainty of absorption depth of less than 1%. The multi-channel scanning technique is subject to small uncertainties due to imperfections of the scanning mechanics within the spectrograph, yielding an error of less than 0.3%. The accuracy of absorption path length is better than 0.5%. The sum of the listed errors limits the overall accuracy of our instrument to a total systematic error of <6.5% (conservative estimate).

4.2. Evaluation of Absorption Spectra: Measurement Limit and Precision

To determine the trace gas concentrations, a least squares fit algorithm is performed whereby all the reference spectra of the trace gases under observation are fitted simultaneously to the air absorption spectrum (Figure 6). On the basis of the known line strength of the reference spectra and on the fit coefficients determined the optical density of the specific absorption and thus the concentration can be calculated.

4.2.1. Evaluation of measurement error. Very often in the literature the statistical error of the fit coefficient is used to define the error of DOAS data. However, this procedure ignores the fact that least squares fit procedures work properly only on data which scatter randomly around the fitted function. As far as DOAS measurements are concerned, this condition is guaranteed only if the residual spectrum (equal to measurement spectrum divided by the fitted function) contains only pure shot noise. In all other cases where spectral structures besides the shot noise are apparent in the residual (i.e., detector specific structures or unrecognized absorption features of unknown trace gases) the content of a particular channel is not independent of adjacted channels. Therefore the true error is significantly larger than

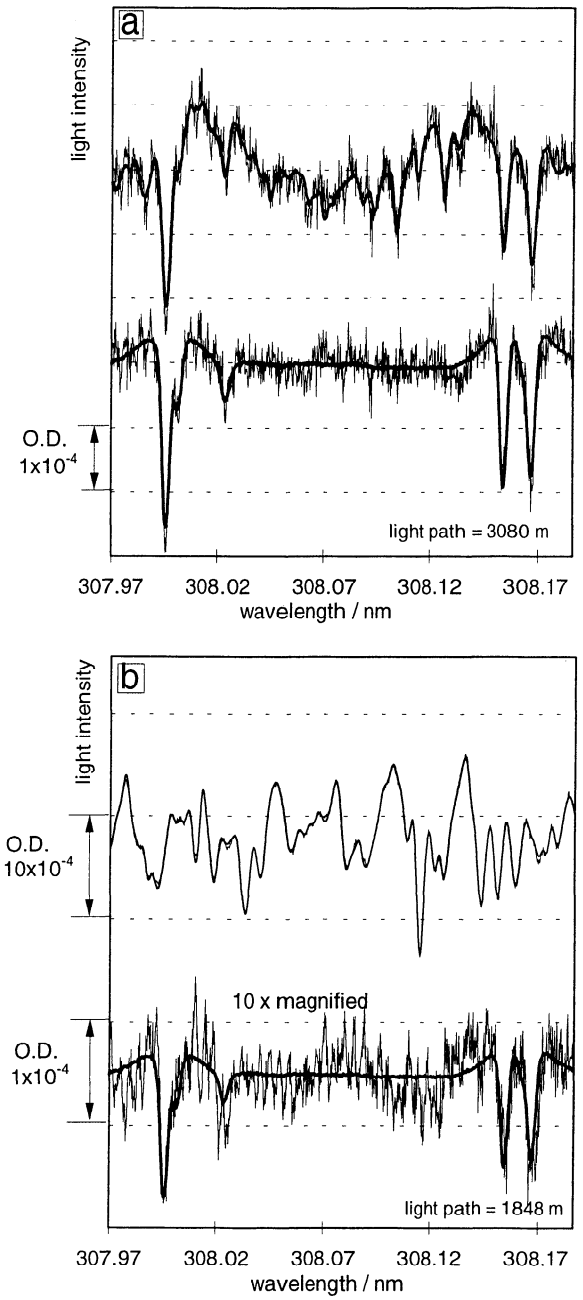

Figure 6. Ambient OH spectra recorded in Pennewitt, Germany, August 16, 1994. Two examples are given. First trace of each panel shows an air spectrum overlaid by simultaneous fit of SO_2, HCHO, $C_{10}H_8$, and OH. The second trace shows the air spectrum after dividing by the fits. (a) The atmospheric spectrum is dominated by OH absorption. The absorption line strength corresponds to [OH]=9.6x10^6 cm^{-3}. (b) A typical case of a spectrum dominated by SO_2 is shown. Here the OH line strength corresponds to [OH]=8.810^6 cm^{-3} (note that vertical grid distance corresponds to an optical density of 110^{-4}). The signal integration times were about 5 min.

indicated by the error of the fit coefficient. Indeed, practice shows that this error calculation is mostly an underestimation (typically by a factor 2 to 4) if the condition of a random channel content distribution in the residual is not fulfilled. Hence the error of the fit coefficients usually cannot be used to determine the uncertainty of atmospheric trace gas measurements. This problem has recently been discussed in more detail by *Stutz and Platt* [1996]. Figure 7 shows examples of residuals of atmospheric spectra for which the corresponding errors by the least squares method are not conclusive. Besides the shot noise, various structures are clearly visible in these spectra.

Residual structures that interfere with the absorption spectrum are of various origins. In addition to absorption structures of unidentified trace gases, other irregular structures occur which are partly self-produced due to weak instabilities of the optical alignment. Other problems result when the spectral shapes of the applied reference spectra do not perfectly fit the apparent absorption. Therefore various methods are used by different investigators to determine the evaluation error. Often these methods may only provide an upper error limit or may be attributed to systematic uncertainties (not shown here). This problem of a comprehensive error evaluation of LP-DOAS spectra is well known and was already addressed during DOAS intercomparison studies reported by *Camy-Peyret et al.* [1994] and *Hofmann et al.* [1995].

4.2.2. Residual inspection by cyclic displacement (RICD). In general, the determination of the statistical error of spectra evaluation assumes knowledge of the apparent statistical distribution function of the residual channel contents. In the case of shot noise this function is known to be described by Poisson statistics. In other cases where irregular structures dominate the apparent residual the individual distribution function is not known. Nevertheless, its effect on the spectra evaluation procedure (least squares fit) has to be considered. Here we present a new method to determine the total spectral evaluation error based on the particular apparent residual.

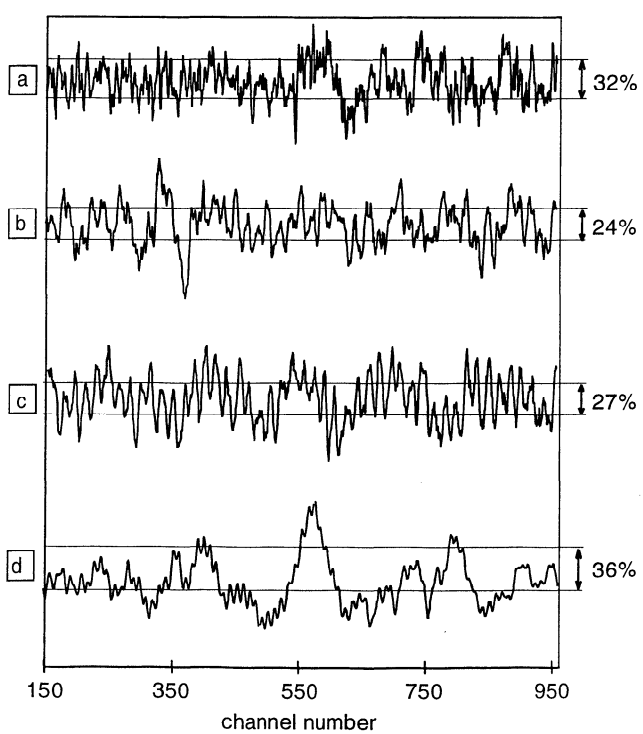

Figure 7. Four extreme examples of in situ residual spectra recorded in Penewitt in August 1994 are shown. The 2σ errors of optical density of OH fit as calculated by equation (4) are indicated. Here values are given in fractions of residual peak-peak structure: (a) 32%, (b) 24%, (c), 27%, and (d) 36%.

The RICD method assumes that each absorption spectrum possesses an individual residual structure that biases the spectral evaluation results. It is further assumed that the spectral positions of these structures are randomly distributed over the spectral range. Obviously, the true residual structure is not known. Therefore, for each individual, measured atmospheric absorption spectrum, an ensemble of "simulated" residuals is created. The simulation of an ensemble of residuals is based on the most probable residual determined by the least squares fit. The total RICD procedure consists of four steps: spectrum evaluation, cyclic displacement, spectra reevaluation, and statistical analysis.

For step (1), the spectrum evaluation, the atmospheric measurement spectrum is evaluated by applying a linear or nonlinear least squares fitting procedure (cp. Figure 6). The corresponding residual is determined by dividing the measurement spectrum by the product of all simultaneously fitted reference spectra. This procedure yields the "best estimate" of the residual. In the next steps the spectral pattern of this residual represents the pattern of the true residual structure. Both the result of fit and the residual is needed for further processing.

Next in step (2), the residual is cyclically displaced by a random number of channels within the spectral range of evaluation (between 1 and maximum number of channels). Thereby the statistical distribution of the channel contents and the residual pattern are maintained, but the position of the residual features with respect to the channel numbers (or wavelength scale) has changed. After cyclic displacement of the residual, the spectral fit obtained in the evaluation step (1) is multiplied with the "new" residual to yield a simulated "new" atmospheric spectrum. It is the first of a number (typcally 100) of simulated spectra which are obtained by displacing the original residual (as described above) by random numbers of channels. Figure 8 shows two new spectra with different displaced residual as examples.

All those simulated spectra are reevaluated in step (3) by performing the entire spectrum fitting procedure (see step (1)).

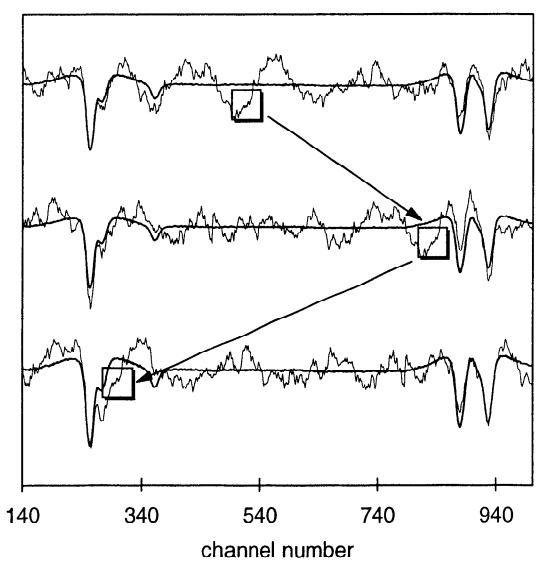

Figure 8. Two examples of spectra with displaced residual as performed by the RICD method. Upper trace shows the entire spectrum plus OH fit. The center trace and the bottom trace show the same spectrum, but the residual is cyclically displaced (indicated by arrows; see text). The corresponding OH fits of reevaluation are superimposed (see text).

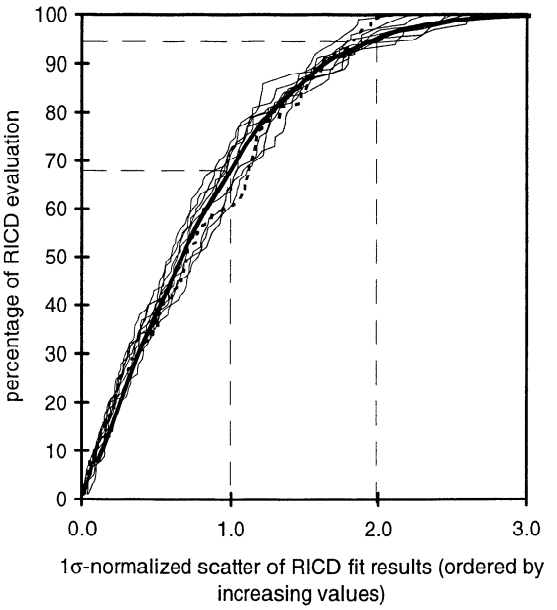

Figure 9. Test of statistical partition of the RICD results scattering around the respective measurement value. The empirical normalized error functions of RICD results (absolute values) are investigated for selected 12 extreme cases of interfering structures (four are shown in Figure 7). The error functions of RICD results (thin lines) run close around the pure Gausian error function (bold line) indicating that the Gausian 2σ value is a suitable error parameter of RICD results. For a pure shot noise residual the same behavior of RICD results can be found (bold dotted line).

This yields a number of new evaluation results (equal to RICD results) that scatter around the best estimate obtained in the first evaluation.

In step (4), statistical analysis is performed on the ensemble of spectral fits. The scatter of the RICD results is taken as a proper measure of the uncertainty of spectra evaluation (the proof is given in a forthcoming paper). Since the statistical partition of the RICD results is of Gaussian-type (see below), the standard deviation of the scatter (equal to 1σ RICD error) describes the evaluation uncertainty, and hence RICD errors have a statistical meaning.

As examples, we show the result of RICD investigations with respect to OH for a selection of 12 different residuals that visually represent extreme cases of residual structures of atmospheric spectra recorded during a field measurement campaign in 1994 (see section 5.2). Four of them are shown in Figure 7. Each residual was investigated by 100 RICD evaluations. Figure 9 shows the cumulative partition function (equal to empirical error function) of the 100 RICD fit results for the 12 selected residuals. In addition, in Figure 9, the error function of a pure Gaussian partition (smooth bold line) is drawn. It can be seen that the error functions of the RICD results are similar to the pure Gaussian line, thus demonstrating the statistical behavior of the RICD results.

In cases when the residual is shot noise, the RICD calculation provides the same error value as determined by the error of fit coefficient. Furthermore, there is no qualitative discrepancy between the error function of a pure shot noise residual and a structured residual (like, e.g., the spectra in Figure 7). One case of pure shot noise residual (bold dotted line in Figure 9)

demonstrates this good agreement. Therefore the RICD method can be applied to pure shot noise residuals, to irregular structured residuals, and to mixed type residuals where shot noise and irregular residual structures are simultaneously apparent.

In principle, the RICD method is not limited to absorption by OH. The RICD method was also applied to SO_2, HCHO, and $C_{10}H_8$ which also absorb within in the wavelength range. Notice that their spectral signature is quite different (cp. Figure 3). This investigation revealed that the statements given for OH are also valid for these species (not shown here).

4.2.3. Significance and limitation of the RICD method. The RICD method inherently considers the total uncertainty of spectra evaluation caused by all "random" type spectral structures like shot noise, instrumental artifacts, and irregular structures of unknown origin. It assumes that all residuals have individual structures and that the peak-to-peak strengths of the residual structures are approximately constant across the complete spectral range of observation.

However, interfering structures may occur systematically, that is, are present in subsequently recorded spectra. With respect to LP-DOAS they can be caused by atmospheric absorption of unidentified species, unremovable instrumental spectral patterns, and bad matches of in situ measurement spectra with reference spectra used. For instance, for our instrument, weak etalon-type structures occur in some spectra. From our first experiences, even for those cases, the RICD error seems to be a suitable measure of evaluation uncertainty. It has to be emphasized that the RICD method does not distinguish between systematic and random structures (since it is based on the individual residuals). Obviously, in the case of systematic structures, the spectra evaluation results deviate systematically from the true value. Thus, in the case of systematic structures, the RICD error can no longer have a statistical meaning and the RICD error has to be treated as a systematic uncertainty.

Furthermore, it may be argued that the RICD method has two specific problems. First, a point of discontinuity can occur in the RICD spectra after the cyclic displacement of the residual. In order to prevent a point discontinuity, the contents of the first and the last channel of the entire spectrum are required to have close values (within the residual noise). Second, a residual as derived from the spectral evaluation could be biased by the evaluation itself. Thus a statistical statement based on the obtained residual may be not valid for the "true residual". Indeed, further investigations of the RICD method based on simulated absorption spectra revealed that the introduced RICD error is slightly underestimated depending on the actual residual. For the atmospheric spectra discussed here a correction factor of 1.15 is needed. The uncertainty of the correction factor and thus the uncertainty of the final RICD error is about 10%. A detailed investigation of the RICD method is discussed in a forthcoming paper.

Precision and detection limit of OH-DOAS spectroscopy can now be defined as absolute precision equal to

$$2\sigma\ (\text{RICD error of OH fit}) \times 1.15 \tag{4}$$

and detection limit

$$\frac{2\sigma(\text{RICD error of OH fit}) \times 1.15}{\text{evaluation result of OH}} = 1 \tag{5}$$

For all the measurements presented here (section 5) the residuals were clearly dominated by random type structures, and RICD errors have a statistical meaning.

5. Experimental Field Studies

5.1. Short Light Path Investigations

Field measurements at very short absorption light path lengths give the opportunity to investigate the spectral "blank" signal of the instrument at real measurement conditions but at negligible atmospheric absorption. For this the MRC can be switched into a four-pass mode yielding a path length of only 154 m. It was found for short integration times (few seconds) that the spectral structures can be identified as pure shot noise: For values of peak-to-peak noise higher than 1×10^{-4} (optical density) the experimental noise was found to be the 1.2-fold value of the calculated theoretical shot noise, corresponding to a minimal detectable optical density of about 2×10^{-5}.

The smallest value that could be observed is a noise-to-signal-ratio of about 3×10^{-5} (peak-peak) even for long integration times (10 min or more). A corresponding minimal detectable optical density is about 1×10^{-5}. These type of spectra show no noise-type structure anymore but show irregular structures that differ for each single spectrum. They were found to be instrumental artifacts of partly known origin, like spectral etalon-type modulations that originate from the lens systems or weak substructures of the spectral laser profile that depend on the stability of the laser system. Because the residual defines the detection limit, a corresponding minimal detectable OH concentration of $[OH]_{MIN} \approx 6\times10^5$ molecules cm^{-3} (for 1.85-km path length) can be theoretically derived for the present instrumental configuration.

5.2. Long Light Path Performance

Extended atmospheric studies were carried out during the field campaign **P**hoto-**O**xidant Formation by **P**lant-Emitted **C**ompounds and **OH** **R**adicals in **N**ortheastern Germany (POPCORN) in August 1994 in Pennewitt, a rural site in northeastern Germany. A detailed description of the studies of POPCORN will be given elsewhere, but it should be mentioned that two different instruments for OH measurements (LIF [*Hofzumahaus et al.*, 1996]) and this instrument [*Dorn et al.*, 1996] were running simultaneously [see *Brauers et al.*, 1996]. The MRC was switched to a path length of 1848 or 3080 m. OH concentrations up to 1×10^7 molecules cm^{-3} were observed. Typical signal integration time was about 5 min.

In continental air, SO_2, HCHO, or $C_{10}H_8$ absorption interfer with the OH absorption spectrum (cp. Figure 3). Thus reference spectra of all the trace gases under observation and an additional polynomial of 7th order were simultaneously fitted to the air spectra to determine the absorption by the individual trace gas, respectively. Corresponding reference spectra were recorded by the use of reference cells. Both reference spectra and air spectra were subjected to the MCST method (cp. section 3.2). Figure 6 gives two examples of air spectra evaluation. Note that the vertical grid distance in Figures 6 corresponds to an optical density of only 1×10^{-4}. The first trace of panels a and b shows an air spectrum overlaid by the product of simultaneously fitted SO_2, HCHO, $C_{10}H_8$, and OH reference spectra. The second trace shows the air spectrum after dividing by the SO_2, HCHO, and $C_{10}H_8$ fit. The air spectrum in panel a is an example of a spectrum dominated by OH absorption. The corresponding OH concentration is 9.6×10^6 molecules cm^{-3}. In panel b a case of strong interference by SO_2 is shown. Here the SO_2 absorption is more than 10 times stronger than the OH absorption

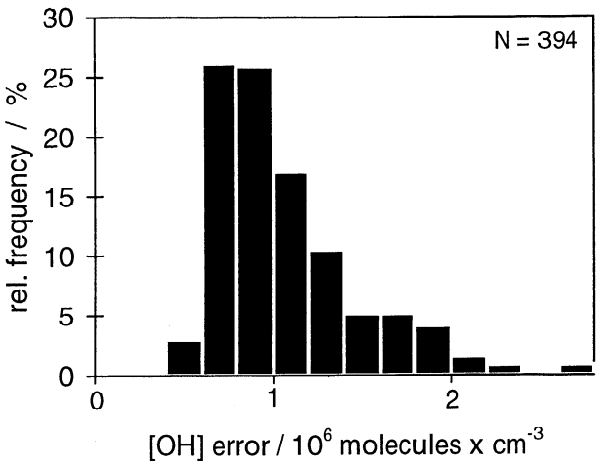

Figure 10. Frequency distribution of the measurement errors (1σ RICD error) of the total number of OH measurements N = 394) recorded during the POPCORN field campaign.

(corresponding to [OH] = 8.8×10^6 molecules cm^{-3}). Even in this case, OH can be unambiguously determined.

An overview over the measurement errors of all the LP-DOAS OH records during the POPCORN field campaign is given in Figure 10. It can be seen that most 1σ measurement errors are below 1×10^6 molecules cm^{-3}. A typical 2σ measurement limit (as defined in section 4.2.3) is about 1.5×10^6 molecules cm^{-3}.

6. Summary and Further Development

The new LP-DOAS instrument for local and absolute OH measurements consists of a picosecond laser system in conjunction with a beam-stabilizing multiple-reflection cell and a high resolution Echelle spectrograph linked to a photo diode array. By combination of the new optical setup and the multi channel scanning technique [*Brauers et al.*, 1995] it was possible for the first time to detect differential optical densities down to 2×10^{-5} using a photo diode array detector. This is 1 order of magnitude lower than previous LP-DOAS systems, which allows to reduce the light path to 2 to 3 km. The instrument was extensively used for OH measurements during a field campaign in northeastern Germany in August 1994 (POPCORN). A detailed error consideration shows that the overall accuracy is better than 6.5%. Furthermore, the new RICD method allows to determine the measurement precision based on individual measurement spectra even in cases where interfering structures beside the shot noise are present in the residual spectra. Under real field measurement conditions a 2σ precision (and detection limit) for OH of typically 1.5×10^6 molecules cm^{-3} is achieved.

Although instrumental spectral artifacts (interfering structures) were reduced by 1 order of magnitude, they are still the limiting factor for many atmospheric measurements. Remaining error sources are the instabilities of the laser light source and to a lesser extent parasitic etaloning in some of the optical components. Moreover, in the present configuration, the need for frequent optical adjustment control results in limitations of time resolution. Further development is focused on minimizing these limitations.

References

Armerding, W., A. Herbert, M. Spiekermann, and F. J. Comes, Laser fast scanning multi-path absorption, an ultrasensitive technique for monitoring tropospheric trace gases, in *Optical Methods in Atmospheric Chemistry*, edited by H. I. Schiff and U. Platt, *Proc. Int. Soc. Opt. Eng., 1715*, 353-360, 1992.

Armerding, W., M. Spiekermann, and F. J. Comes, OH multipass absorption: Absolute in situ method for local monitoring of tropospheric hydroxyl radicals, *J. Geophys. Res., 99*, 1225-1239, 1994.

Brandenburger, U., Aufbau und Charakterisierung eines hochauflösenden Laser- Langpfad- Absorptionspektrometer, Diploma-Thesis, KFA Jülich and University of Bonn, 1992.

Brauers, T., M. Hausmann, U. Brandenburger, and H.-P. Dorn, Improvement of differential optical absorption spectroscopy using multi-channel-scanning-technique, *J. Appl. Opt., 34*, 4472-4479, 1995.

Brauers, T., U. Aschmutat, U. Brandenburger, H.-P- Dorn, M. Heßling, A. Hofzumahaus, F. Holland, C. Plass-Dülmer, and D. H. Ehhalt, Intercomparison of tropospheric OH radical measurements by multiple folded long-path laser absorption and laser induced fluorescence, *Geophys. Res. Lett., 23*, 2545-2548, 1995.

Callies J., Absorptionsspektroskopischer Nachweis von Hydroxyl-Radikalen in der Troposphäre, PhD.-Thesis, KFA Jülich and University of Cologne, Cologne, Germany, 1988.

Camy-Peyret, C., et al., Intercomparison of instruments for tropospheric measurements using differential optical absorption spectroscopy, *J. Atmos. Chem., 23*, 51-80, 1996.

Crosley D. R., Local measurements of tropospheric HO_x, *NASA Conference publication, 3245*, 1994

Dorn, H.-P., J. Callies, U. Platt, and D. H. Ehhalt, Measurement of tropospheric OH concentrations by laser long-path absorption spectroscopy, *Tellus, Ser. B., 40*, 437-445, 1988.

Dorn, H.-P., R. Neuroth, T. Brauers, U. Brandenburger, and D. H. Ehhalt, Measurement of tropospheric OH radical concentration by differential UV laser long path absorption, in *Optical Methods in Atmospheric Chemistry*, edited by H. I. Schiff and U. Platt, *Proc. Int. Soc. Opt. Eng., 1715*, 361-366, 1992.

Dorn, H.-P., R. Neuroth, and A. Hofzumahaus, Calculation and accuracy of the OH line absorption coefficient. Implications for tropospheric long-path absorption measurements, *J. Geophys. Res., 100*, 7397-7409, 1995a.

Dorn, H.-P., U. Brandenburger, T. Brauers, and M. Hausmann, A new in situ laser long-path absorption instrument for the measurement of tropospheric OH radicals, *J. Atmos. Sci., 52*, 3373-3380, 1995b.

Dorn, H.-P., U. Brandenburger, T. Brauers, M. Hausmann, and D. H. Ehhalt, In situ detection of tropospheric hydroxyl radical concentrations by folded long-path laser absorption. Results from the POPCORN fiel campaign in August 1994, *Geophys. Res. Lett., 23*, 2537-2540, 1996.

Ehhalt, D. H., H.-P. Dorn, and D. Poppe, The chemistry of the hydroxyl radical in the troposphere, *Proc. R. Soc. Edinburgh, Sect. B, 97*, 17-34, 1991.

Gomer, T., T. Brauers, F. Heintz, J. Stutz, and U. Platt, *MFC Version 1.98 User Manual*, Univ. of Heidelberg and KFA Jülich, Heidelberg, Germany, 1993.

Hewitt, C. N., and R. M. Harrison, Tropospheric concentrations of the hydroxyl radical - A review, *Atmos. Environ., 19*, 545-554, 1985.

Hofmann, D., et al., Intercomparison of UV/visible spectrometers for measurements of stratospheric NO_2 for the network for the detection of stratospheric change, *J. Geophys. Res., 100*, 16765-16791, 1995.

Hofzumahaus, A. H.-P. Dorn, J. Callies, U. Platt., and D. H. Ehhalt, , Tropospheric OH concentration measurements by laser long-path absorption spectroscopy, *Atmos. Environ., Part A, 25*, 2017-2022, 1991.

Hofzumahaus, A., U. Aschmutat, M. Hessling, F. Holland, and D. H. Ehhalt, The measurement of tropospheric OH radicals by laser-induced flourescence spectroscopy during the POPCORN filed campaign, *Geophys. Res. Lett., 23*, 2541-2544, 1996.

Hübler, G., D. Perner, U. Platt, A. Torrissen and D. H. Ehhalt, Grundlevel OH radical concentration: New measurements by optical absorption, *J. Geophys. Res., 89*, 1309-1319, 1984.

Mount, G. H., The measurement of tropospheric OH by long path absorption, 1. Instrumentation, *J. Geophys. Res., 97*, 2427-2444, 1992.

Perner, D., U. Platt, M. Trainer, M., G. Hübler, J. Drummond, W. Junkermann, J. Rudolph, B. Schubert, T. Volz, D. H. Ehhalt, K. J. Rumpel, K. J., and G. Helas, Measurement of tropospheric OH concentrations: A comparison of field data with model predictions, *J. Atmos. Chem., 5*, 185-216, 1987.

Platt, U., Differential optical absorption spectroscopy, in *Air Monitoring by Spectroscopic Techniques* , edited by M. W. Sigrist, 27-83, John Wiley, New York, 1994.

Platt, U. and M. Hausmann, Spectroscopic measurements of the free radicals NO_3, BrO, IO, and OH in the troposphere, *Res. Chem. Intermed.*, *20*, 557-578, 1994.

Platt, U. and D. Perner, Direct measurements of atmospheric CH_2O, HNO_2, O_3, NO_2, SO_2, by differential optical absorption in the near UV, *J. Geophys. Res.*, *85*, 7453-7458, 1980.

Platt, U., M. Rateike, W. Junkermann, J. Rudolph, and D. H. Ehhalt, New tropospheric OH measurements, *J. Geophys. Res.*, *93*, 5159-5166, 1988.

Ritz, D., M. Hausmann, and U. Platt, An improved open path multi-reflection cell for the measurement of NO_2 and NO_3, in *Optical Methods in Atmospheric Chemistry*, edited by H. I. Schiff and U. Platt, *Proc. Int. Soc. Opt. Eng.*, *1715*, 200-211, 1992.

Stutz, J. and U. Platt, Numerical analysis and error estimation of differential optical absorption spectroscopy measurements with least squares methods, *J. Appl. Opt.*, *35*, 6041-6053, 1996.

White, J. U., Very long optical paths in air, *J. Opt. Soc. Am.*, *66*, 411-416, 1976.

U. Brandenburger, T. Brauers, H.-P. Dorn, and M. Hausmann, Institut für Atmosphärische Chemie, Forschungszentrum Jülich GmbH, ICG-3, D-52425 Jülich, Germany
(e-mail: m.hausmann@kfa-juelich.de)

(Received June 18, 1996; revised January 24, 1997;
accepted January 24, 1997.)